

Twin domain structure in magnetically doped topological insulators

Jakub Šebesta,^{1,*} Karel Carva,¹ Dominik Kriegner,^{2,3} and Jan Honolka²

¹*Charles University, Faculty of Mathematics and Physics,
Department of Condensed Matter Physics, Ke Karlovu 5 121 16 Praha 2, Czech Republic*

²*Institute of Physics, Academy of Science of the Czech Republic,
Čukrovarnická 10, 162 00 Praha 6, Czech Republic*

³*Institute of Solid State and Materials Physics, Technical University of Dresden, 01062 Dresden, Germany*

(Dated: October 26, 2020)

Twin domains are naturally present in the topological insulator Bi_2Se_3 and affect strongly its properties. While studies of its behavior for ideal Bi_2Se_3 structure exist, little is known about their possible interaction with other defects. Extra information are needed especially for the case of artificial perturbation of topological insulator states by magnetic doping, which has attracted a lot of attention recently. Employing ab initio calculations based on layered Green's function formalism, we study the interaction between twin planes in Bi_2Se_3 . We show the influence of various magnetic and non-magnetic chemical defects on the twin plane formation energy and discuss the related modification of their distribution. Furthermore, we examine the change of dopants' magnetic properties at sites in the vicinity of a twin plane, and the dopants' preference to occupy such sites. Our results suggest that twin planes repel each other at least over distance of 3 – 4 nm. However, in the presence of magnetic Mn and Fe defects a close TP placement is preferred. Furthermore, calculated twin plane formation energies indicate that in this situation their formation becomes suppressed. Finally, we discuss the influence of twin planes on the surface band gap.

Keywords: topological insulators; magnetic doping; native defects; ab-initio

I. INTRODUCTION

One of the most characteristic representatives of topological insulators (TI) are three dimensional time reversal symmetry (TRS) protected TIs [1–4]. Although the bulk band structure contains a band gap, the surface of such materials hosts unique conductive states, which intersect in the so-called Dirac point possessing a linear dispersion [1, 4–7]. Formation of surface electron states originates from the strong spin orbit coupling (SOC), which stems from the occurrence of heavy elements as *e.g.* Bi, Se or Te and the presence of TRS. It ensures band crossing at high symmetry points of the Brillouin zone [8, 9], while no extra crystal symmetry is required (compare *e.g.* topological crystal insulators [1, 5]). Combination of strong SOC and TRS leads to the spin polarization of surface bands [3, 5, 8]. Electrons occupying states in the proximity of the Dirac cone with an opposite momentum possess also opposite spins, so-called spin-momentum locking. It ensures *e.g.* suppression of back-scattering and related outstanding surface transport properties [9, 10].

In real applications the influence of defects could be important, since they might significantly alter properties of the ideal matter. They could be varied intentionally by chemical doping. In the case of TIs it includes particularly magnetic doping. It leads to breaking of TRS and therefore it opens a surface gap [11, 12]. Then, not only does a possible control of the surface conductivity appear due to increased surface scattering, but also it

could bring about the occurrence of new unique phenomena *e.g.* QAHE [13]. Besides, native defects occur there, naturally. Their presence is hardly controllable and they might have a significant impact on physical properties [14, 15] as well. There could exist several kinds of native defects depending on the actual compound and the growth process. These include twin planes (TP), which are the focus of this article.

An important group of 3D topological insulators are bismuth chalcogenides, such as Bi_2Se_3 [16, 17] which have been shown to be prone to the formation of twin domains [18, 19]. This compound possesses a relatively simple band structure, convenient for experimental and theoretical studies, with a Dirac cone appearing at the Γ point. The crystal structure of Bi_2Se_3 , belonging to the $R\bar{3}m$ space group, consists of Bi and Se hexagonal layers. They are gathered into quintuple layers (QLs), in which Bi and Se layers alter (Figure 1). Due to the coupling of QLs only by van der Waals (vdW) forces there appears a gap between QLs, so-called ‘van der Waals’ gap [17]. The presented crystal structure offers several sites, which could be occupied by magnetic atoms. Based on the theoretical and experimental studies the most probable position occupied by a magnetic dopant (Cr, Fe, or Mn) is the substitutional position, where magnetic atoms replace Bi ones [20–22]. Recently, a formation of septuple layers induced by magnetic defects was described. However, it was shown that it is negligible in Bi_2Se_3 for small concentrations of magnetic dopants [23]. In our calculation we employ especially Mn^{Bi} as well as Fe^{Bi} magnetic dopants. Naturally, there also appear native defects like Bi or Se anti-sites (Bi^{Se} resp. Se^{Bi}), where Bi atoms replace Se ones and *vice versa*. This non-stoichiometry arises due to difficulties in controlling growth conditions,

* Corresponding author: sebesta.j@email.cz

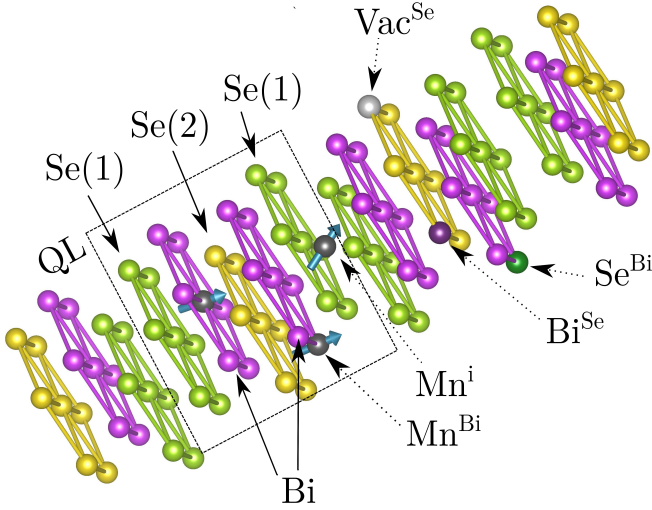


FIG. 1: Layered crystal structure of Bi_2Se_3 . Se and Bi layers gathered into QLs are depicted. Examples of (non)-magnetic defects are shown: (Mn^{Bi}) substitutional Mn atoms, (Mn^{i}) interstitial Mn atoms, (Bi^{Se}) resp. (Se^{Bi}) Bi and Se anti-sites, (Vac^{Se}) Se vacancies.

which result in Bi- or Se- rich samples [20, 24–27].

The above mentioned TPs represent a stacking fault of the layered structure of bismuth chalcogenides [18, 19, 28]. Their ideal structure contains three possible stacking positions of hexagonal layers alternating similarly to the FCC stacking sequence. During the formation of the crystal there exist two energetically almost equivalent sites, which the atoms in the new layer can choose to occupy. Therefore, mirrored stacking might arise, which could be represented by a 60° rotation of new layers in relation to the ideal ones [19]. It results in the inverse order of the *abc*-like stacking beyond the TP (Figure 2). Possibly, there exist a few positions where TP could occur, but the most probable ones lie at outer chalcogenides of quintuples [29]. This means that stacking order inside each separate QL contains no defect, the perturbation occurs in the vdW gap between them. QLs after the TP are then constructed with a mirrored stacking order (Figure 2). The reported experiments show that the presence of TPs strongly depends on the used substrate [30, 31].

Similarly to point defects, TPs might have a significant influence on the physical properties [32]. Therefore, in this paper we focus on the influence of TPs on 3D TI Bi_2Se_3 behavior and their interplay with chemical disorder, especially the magnetic one. Primarily, we describe a distribution of TPs in a nanoscopically thin Bi_2Se_3 slab. Then, we discuss their behavior under the presence of magnetic and non-magnetic dopants. Finally, the influence of TPs on the surface states is shown.

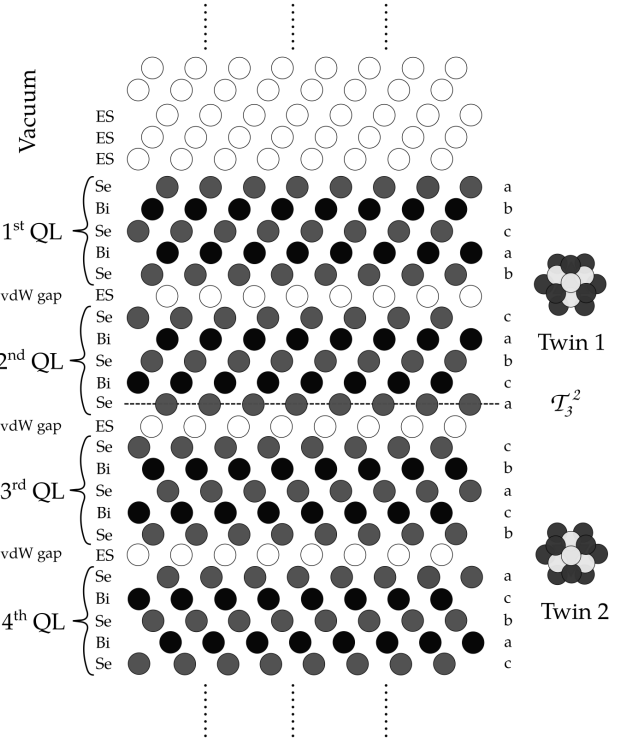


FIG. 2: Layout of the simulated multilayer Bi_2Se_3 structure including twin planes. Proportions of atoms are neglected. QL – quintuple layer, ES – empty sphere, T_3^2 twin plane between the second QL and the third QL.

II. FORMALISM

The study employs ab-initio calculations done in the framework of the tight-binding linear muffin-tin orbital method within the atomic sphere approximation (TB-LMTO-ASA) formulated in terms of Green's functions [33, 34]. It involves the local spin density approximation with the Vosko-Wilk-Nursain exchange-correlation potential [35] and using of a *s,p,d* atomic model. Calculations were treated in the scalar relativistic approximation, where on-site spin-orbit coupling was involved into the scalar relativistic Hamiltonian as a perturbation. A basic screened impurity model was included to improve treating electrostatics of disordered systems [36]. Thanks to using of the Green's function formalism chemical disorder could be included by the coherent potential approximation (CPA) [37]. It allows to avoid using of large statistical ensembles and it is suitable for small perturbation in the system. To simulate a layered structure, where it is important to treat TPs, layered Green's functions reflecting translation symmetry only within an atomic layer were employed [34, 38–40]. In calculations, a multilayer system is attached to the semi-infinite leads, which have to satisfy self-consistent conditions. Due to the coupling of the multilayer to the attached leads it is possible to obtain a self-consistent

solution also for the inner layers. Based on the down-folding method one is able to construct recursively embedding potentials acting from both sides on the particular layer, which are related to the interlayer coupling. For a detailed description we refer the reader to Ref. [34, 38].

The crystal structure is based on experimental lattice parameters (Bi_2Se_3 unit cell $a = 4.138 \text{ \AA}$ and $c = 28.64 \text{ \AA}$ [17]), which were used to build Bi_2Se_3 multilayer structures. The vdW gap in between QLs is included within ASA by placing appropriate empty spheres (ES). To avoid effects of the substrate (or leads) and to concentrate only on the behavior of proper Bi_2Se_3 layers we surround it by vacuum, which is treated in a similar sense to the vdW gap. It is formed from the fcc-like stacked empty sphere layers keeping the three-fold symmetry of Bi_2Se_3 layers. Further, because leads should fit to the simulated structure slightly modified scandium is selected. Its hcp crystal structure suits to fcc like stacking within QLs and it possesses not too much distinct lattice parameters [41]. However, leads are more less unimportant thanks to used vacuum spacers.

Finally, one is able to construct a layer structure, which consists of intermediate Sc layers at borders, coupled to semiinfinite leads, and several Bi_2Se_3 QLs enclosed by the vacuum spacer. In our calculation we employed ten or twenty QLs wide Bi_2Se_3 structures and the vacuum spacers about ten ES layers width. These dimensions are sufficient to simulate the vacuum and to obtain surface gapless states. Native defects (Bi^{Se}) as well as magnetic either Mn^{Bi} or Fe^{Bi} doping are included. In general, we assumed homogeneous disorder, where mentioned defects occupy the appropriate sites with the same probability, unless otherwise stated. This assumption is supported by synchrotron experiments which show that Mn is not metallic in Bi_2Se_3 and thus does not segregate there [42]. The influence of the defects on the crystal structure is reflected by local lattice relaxation similar to previous bulk calculation of Bi_2Te_3 and Bi_2Se_3 [14, 43]. However, the relaxation corresponding to the presence of surfaces is not included there. In our calculation we simulate TPs in the vdW gaps with respect to the required 2D periodicity in the layer. Hence no structure boundaries within a layer, which are related to the presence of TP [28], are involved.

The selected approach unfortunately introduces numerical artifacts within the employed TB-LMTO-ASA framework, which renders calculations of absolute formation energy of an extra stacking fault not reliable. Therefore, we deal only with relative formation energy considering the same number and similar type of stacking faults, while we focus on various composition and TPs distribution. Furthermore, the systematic error depends on the distance of the twin plane from the surface as discussed in the Appendix. The dependence obtained there is thus subtracted from data presented in Results where applicable. Since we deal with various positions of TPs within the multilayer sample we describe their location by sub- and superscript denoting adjacent QLs for

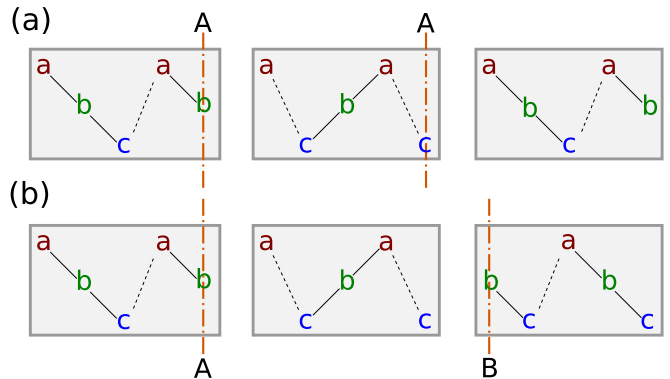


FIG. 3: Twin plane orientation. There exist two mutual orientation of TPs. The first, TPs are located at the same sides of QLs (similar letters – AA resp. BB). The second, TPs occurs at the different sides of QLs (distinct letters – AB).

clarity. The notation \mathcal{T}_{x+1}^x is used for simplicity, where QLs are enumerated from the top interface.

III. RESULTS AND DISCUSSION

Stacking fault energies related to TP formation in ideal Bi_2Se_3 have already been studied elsewhere [28, 29]. Here we focus on their mutual interaction within Bi_2Se_3 slabs and subsequently on their interplay with chemical disorder.

A. Inter twin plane interactions

1. Structure without disorder

One of the simplest ways to study interactions between TPs is the introduction of two TPs in the pristine Bi_2Se_3 multilayer structure. Keeping the position of one TP fixed while another one being independent allows us to determine corresponding relative formation energies over all possible mutual positions of TPs (Figure 4). When studying multiple TPs we have to consider that TPs can occupy the same or distinct sides of particular QLs (Figure 3). Different possible cases are compared in Section III D. In the remaining text we show for clarity the simplest case with identical orientations of TPs (denoted as AA according the Figure 3, resp. AAA in the case of two extra TPs). This situation represents qualitatively well the most probable behavior as it also resembles the lowest energy case of systems with non-identical TPs (Section III D).

Considering two TPs in the multilayer structure consisting of 10 QLs, we find that the dependence related to a single TP, discussed in details in the Appendix (Figure 13), is changed almost only for adjacent TPs, where an extra interaction energy appears (Figure 4). However,

for such a small multilayer structure it is not convenient to study TP interactions because of the strong interplay with the interfaces, which is shown in the Appendix (Figure 13a). It is reflected in bending of calculated energy dependencies (Figure 4) caused by non-negligible energy contribution originating from the interactions between TPs and vacuum interfaces (Figure 13).

Therefore, we introduce a larger structure consisting of 20 Bi_2Se_3 QLs, where positions of two border TPs are fixed and the third one is able to move in between them (Figure 5a). This allows us to study the behavior of a TP in a more realistic situation where it is affected primarily by other surrounding TPs rather than a surface. Interface proximity effects are thus reduced in this situation.. The 3 TP calculation again shows a clearly visible repulsion of neighboring TPs (Figure 5a), especially after the subtraction of the surface induced contribution to single TP energy (Fig 13). It reveals the occurrence of a significant interaction energy contribution appearing for TPs distant up to the length of three QLs. This suggests that TPs in a pure sample are likely spread over the sample with mutual distances which exceed at least the width of three or four QLs. Experiments utilizing X-ray nanobeam microscopy prove that if more TPs are observed, they are clearly several 10 nm apart [19]. Hence, one can compare it with the width of one QL, which is about 1 nm [17]. Nonetheless, one should be aware that we are comparing ground state calculations with a molecular beam epitaxy growth, which occurs far from equilibrium conditions.

2. Native and magnetic defects

The interaction between TPs significantly changes when chemical disorder is introduced in the sample. For all studied types of doping (Mn^{Bi} shown in Figure 5b, or Se^{Bi} shown in Figure 5c) we observed a modification of the dependence of the relative formation energy on the distributions of TPs in comparison to the pure sample (Figure 5a). Thanks to the presence of disorder the monotonous dependence on the distance from a certain vacuum interface disappears (compare Figs. 5b,c to Figure 5a; \otimes -, \boxtimes -points). Moreover, the observed relative energy differences are almost one order of magnitude smaller (Figure 5b,c). It may be caused by suppressed interactions between TPs compared to the ideal case. The presence of a TP apparently does not represent such significant perturbation in disordered systems as it does in the case of pure, regular systems.

Calculations show that a system with magnetic disorder (Mn^{Bi}) prefers gathering of TPs (Figure 5b) instead of their spreading observed in the undoped system. On the other hand, non-magnetic disorder rather maintains a repulsion between TPs, although it is quite weak (Figure 5c) in comparison to the ideal case (Figure 5a), and it is non-negligible only for adjacent TPs. This indicates a significance of magnetism related effects, although we

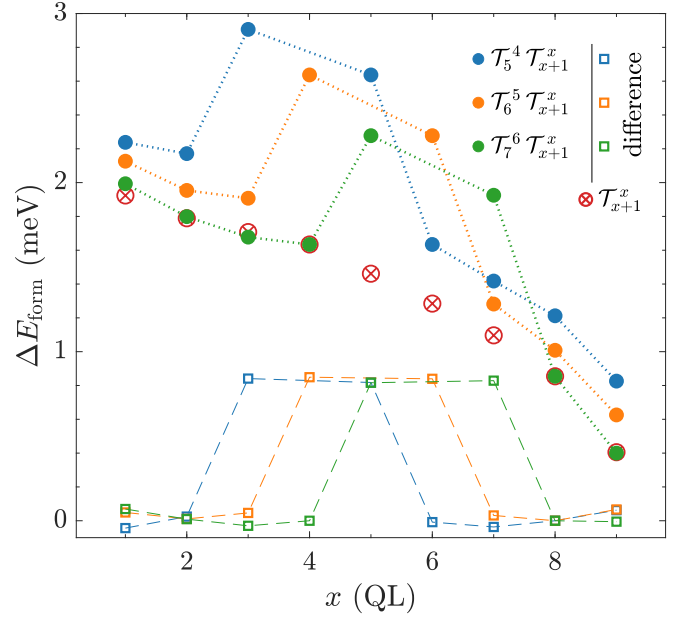


FIG. 4: (●) Relative formation energy of two TPs in dependence on their position within the structure, which consists of 10 Bi_2Se_3 QLs. (\otimes) Relative formation energy of a single TP is depicted for comparison. Relative formation energies belonging to the different numbers of TPs are related to distinct absolute energies. (\square) Energy curves associated to two TPs with subtracted single TP curve contribution.

cannot exclude the role of different chemistry between dopant species. Therefore we study the influence of the magnetism in more detail in next sections.

B. Twin plane formation under chemical disorder

We have calculated dependencies of the relative formation energy of TPs on the concentration x of magnetic Mn^{Bi} or Fe^{Bi} and native Se^{Bi} defects to describe the influence of the defect presence on the tendency to TP formation. (Figure 6).

The calculated relative formation energy, obtained for different number of included TPs concerning also their distinct positions, almost linearly grows with the increasing concentration of magnetic defects. It proves that increased amount of magnetic dopants x leads to the suppression of TPs in the multilayer. On the other hand the non-magnetic disorder (Se^{Bi}) decreases the relative formation energy of TPs in the structure. However, the appropriate dependencies exhibit linear behavior as well.

We assume that the suppression of TPs with respect to the increasing concentration of magnetic dopants corresponds to the observed tendency to gathered TPs in the case of magnetic doping (Figure 5b). We suppose that gathering of TPs likely minimize an induced effect on the electron structure, which arises from the interplay

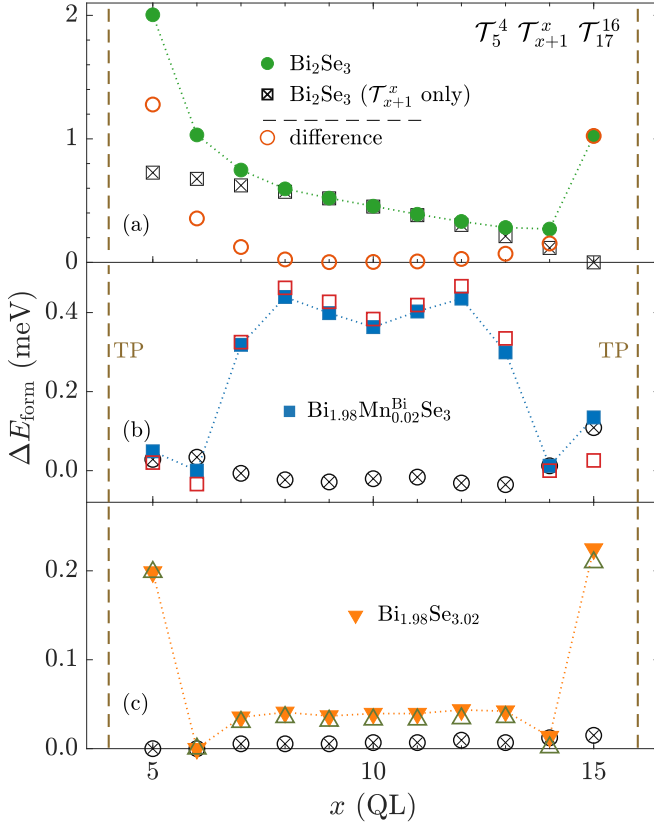


FIG. 5: (●,■,▼) Relative formation energy of three TPs as a function of the position x of the middle TP. Positions of border TPs are fixed. The Bi_2Se_3 multilayer consists of 20 QLs. (a) pure system without any disorder. (b) system with homogeneous magnetic doping. (c) system under presence of homogeneously distributed nonmagnetic disorder. (⊗,⊠) Relative formation energy related to a single TP depicted for comparison. (○,□,△) Energy curves associated to three TPs with subtracted single TP curve contribution. Particular relative formation energy curves are related to different absolute energies.

of TPs and disorder in connection with the magnetism. It agrees with the observation that TPs are less favorable in the magnetically doped systems (Figure 6). Analogously, the fact that the presence of non-magnetic disorder does favor an occurrence of TPs (Figure 6) can be related to the suppressed impact of TPs on the system in that case (Figure 5c). Besides, one might note a proportionality of the relative formation energy to the number of the occurring TPs. It is confirmed by the comparison of the formation energy per single TP (Figure 6).

So far, we discussed ferromagnetically (FM) ordered magnetic dopants. Now, for a moment, we introduce paramagnetic state represented by the disordered local moment (DLM) model in order to decide whether the TP formation energy depends on the type of the magnetic order. In general, these two magnetic phases stand for the

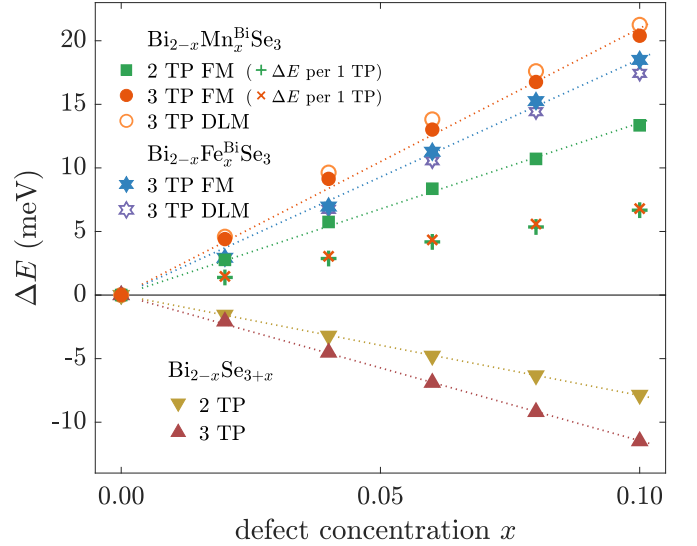


FIG. 6: Relative change of the TP formation energy ΔE in dependence on the concentration of defects x . Structures either with two (\mathcal{T}_8^7 , \mathcal{T}_{13}^{12}) or three TPs (\mathcal{T}_5^4 , \mathcal{T}_{10}^9 , and \mathcal{T}_{17}^{16}) within multilayer consisting of 20 QLs were used. Dependencies under presence of magnetic and native defects are depicted. (+) and (×) denotes hypothetical relative formation energy related to a single TP. Dotted lines depict calculated linear fits.

limiting cases of the magnetic order. One describes a perfectly ordered system, the other one an absolute disorder. One can observe that calculations exhibit only slight changes of the formation energy with a respect to the former FM order. It indicates that the formation energy likely hardly depends on the type of the magnetic order. More precisely, TPs become more favorable in the case of Fe doping. On the other hand, Mn doping illustrates an opposite behavior. We suppose that different slopes of energy dependencies induced either by Mn or by Fe dopants are likely related to different magnitudes of local exchange splitting. Calculations show that Fe atoms bear about $0.8 \mu_B$ smaller magnitudes of magnetic moments than the Mn ones. Therefore, one might assume that the TP formation energy likely scales with the size of the change of the local exchange splitting caused by the mirrored crystal structure.

The mentioned quite large difference between the magnitudes of Fe and Mn magnetic moment stems from a distinct character of the magnetic exchange interactions (Figure 7), where they are evaluated by employing the Liechtenstein formula [43–45]. A comparison shows that unlike Mn related interactions, which are nearly positive except the nearest ones, the exchange interactions between Fe dopants are predominantly antiferromagnetic [46], regardless of the considered magnetic sublattices.

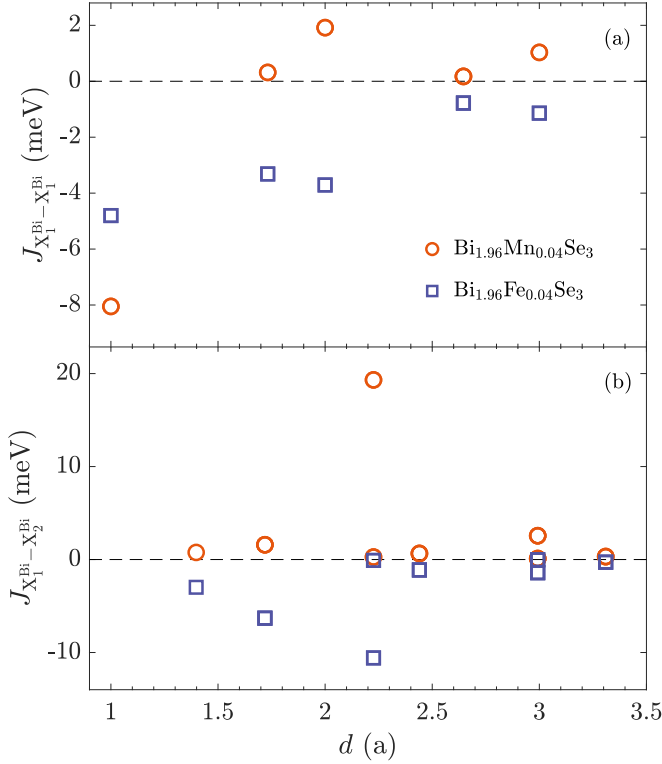


FIG. 7: Exchange interaction between magnetic atoms at the substitution position within Bi_2Se_3 as a function of the distance in units of the lattice parameter a .

Multilayered structures composed of 20 QLs and FM ordering are employed. Exchange interactions at central QLs are evaluated. (a) Exchange interaction within the same sublattice. Interactions within the atomic layer are depicted only in case of layered material. (b) Exchange interaction between atoms occupying different sublattices. Interactions over the vdW gap for the layered material are depicted only.

C. Magnetic dopants behavior

Next, we focused on the influence of TP on the behavior of magnetic dopants, and we calculated relative formation energies of Mn dopants as a function of the position of the dopant determined by indices of the Bi site and QL (Figure 8a). Only one Bi site in the whole structure is partly substituted by Mn. Comparing the shape of corresponding curves differing in the presence of a TP, one observes a clear variation of the relative formation energy caused by the TP. Dependencies without TPs bear a nearly symmetrical behavior, where a deviation is likely caused by an asymmetry of Bi sites concerning the QL structure. The occurrence of the TP modulates the shape of the former energy dependencies as particular sites become relatively more favored or disfavored according to their location with respect to the TP. A comparison of the formation energies (Figure 8a) with the magnitudes of induced magnetic moments on

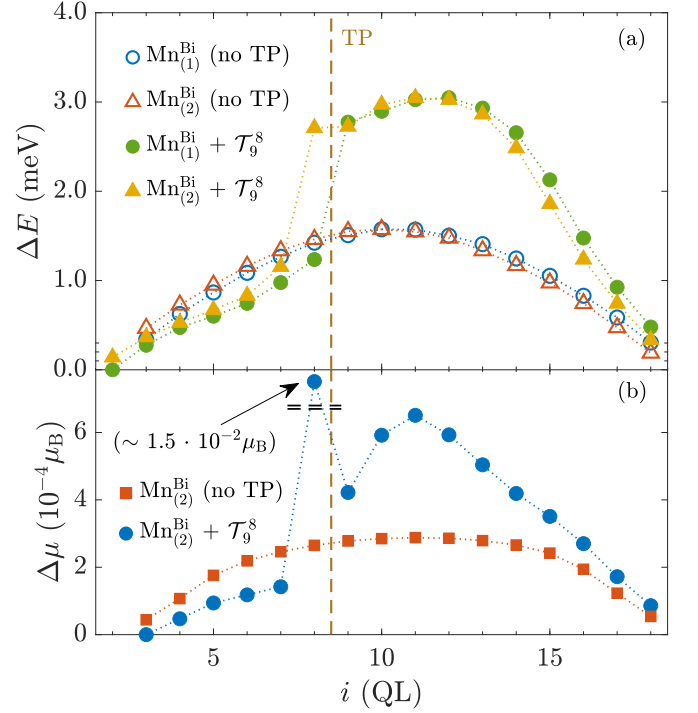


FIG. 8: Layered magnetic doping of the Bi_2Se_3 multilayer. (a) Relative formation energy of Mn^{Bi} substitution defects in dependence on the doped QL i . $\text{Mn}_{(1)}^{\text{Bi}}$ and $\text{Mn}_{(2)}^{\text{Bi}}$ stand for substitutions at distinct Bi sites. $\text{Mn}_{(1)}^{\text{Bi}}$ faces neighbouring QL with lower x . Dependencies with and without TP are depicted. For clarity, they are shifted to fit at the end points. (b) Distribution of magnitudes of Mn^{Bi} magnetic moments in dependence of the position of the substitution i . Only one Bi site labeled by the index i of the appropriate QL is doped by 1% of Mn.

Mn dopants (Figure 8b) indicates a possible relation between the magnetism or spin splitting and the distribution of the relative formation energy of magnetic dopants. One can observe that the effectively suppressed relative formation energies, compared to the ideal structure, correspond to the weakening of induced magnetic moments, and vice versa (Figure 8b). The exceptional change of the magnitude of the magnetic moment, which is about two orders of magnitude larger than the other ones, stems from the proximity of the TP and it can be ascribed to the large charge transfer observed in the undoped structure as described in the Appendix (Figure 14).

The described interplay of TPs and magnetic defects could explain the energetic gain observed for gathered TPs in a magnetic material (Figure 5). Close TPs lead to a smaller perturbation of the whole electronic structure. This might be deduced from the distribution of calculated magnitudes of magnetic moments in a homogeneously doped multilayer as a function of the positions of incorporated TPs (Figure 9a). We see that the closer TPs are, the smaller is the overall variation of magnitudes

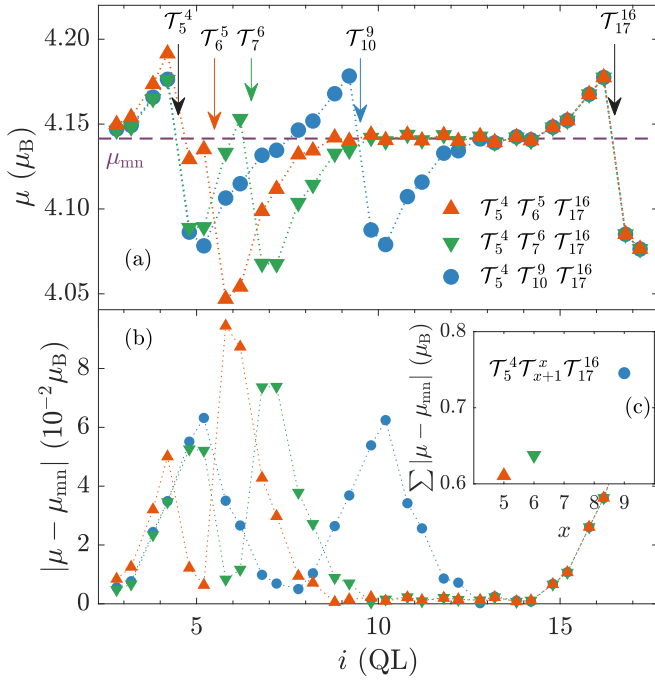


FIG. 9: (a) Distribution of magnitudes of magnetic moments in homogeneously magnetically doped $\text{Bi}_{1.98}\text{Mn}_{0.02}\text{Se}_3$ for various positions of TPs. Mn^{Bi} are labeled by the index i of the appropriate QL. Arrows point positions of introduced TPs. The outer TPs have fixed position in all the cases (black arrows). Whereas, the inner one is being moved, where the color of the arrow corresponds to the color of the dependence. (b) The absolute value of the change of the magnetic moment with the respect to the mean moment value μ_{mn} . (c) The sum of the magnetic moment changes from the previous subplot.

of magnetic moments (Figure 9c).

D. Comparison of different TP orientations

In the previous part we described the simplest case consisting in the identical orientations of three TPs (AAA) (Figure 3). Now, we focus on the influence of nonidentical TPs on the preceding result. To examine it, we invert the orientation of each TP in the former three-TP structures, namely the orientations *BAA*, *ABA*, *AAB* are used (Figure 3), and we calculate the distribution of the formation energy.

We recall that in our approach we are not able to compare well the formation energies of the former identically oriented TPs with the case containing a single TP with the inverted orientation. However, the mutual comparison of the new structures is feasible (Figure 10). Concerning the undoped structure, one can observe that for the studied number of TPs their formation energy strongly depends on the order of TP-type (Figure 10a). Consider-

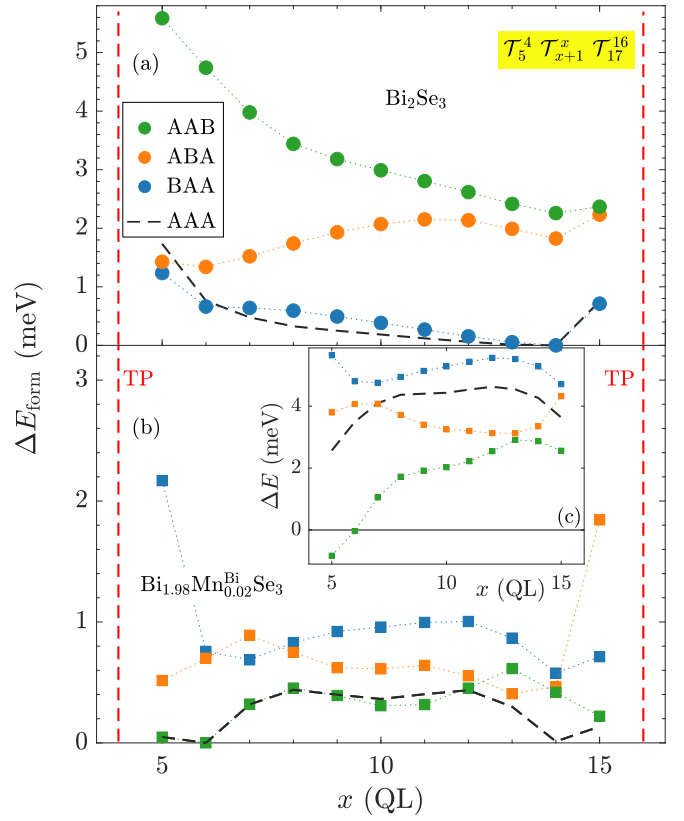


FIG. 10: Dependence of the relative formation energy of three TPs on the position of the middle TP x . Different mutual orientations of the TPs are used. The orientation of TP is labeled by letters A and B. (a) undoped structure. (b) magnetically doped structure. (c) change of the TP formation energy caused by presence of the magnetic defects – $\text{Bi}_{1.98}\text{Mn}_{0.02}\text{Se}_3$ with respect to the undoped case. The relative formation energy curve related to identical TPs (AAA - dashed lines) depicted in panels (a,b) serves only as a shape reference.

ing an increasing index of QLs, it is evident that the *BA* order of two TPs, representing TPs at opposite QL sites (Figure 3), is more favorable than the *AB* one, which stands for TPs at adjacent QL site. Namely, the *BAA* order, containing no *AB* sequence, has the lowest relative formation energy. Besides, it is clearly illustrated at “touching points”, where two adjacent TPs, either *A* or *B* type, are switching (Figure 10a), and the *AB* order with the *BA* one are interchanged (Figure 11). One can assume that the energy difference originates from the mentioned asymmetrical influence of TPs on the surrounding (Figure 8), which differentiate the *AB* and *BA* order. One can notice that the type of the TP sequence can be characterized by number of the vdW gaps in between TPs with the respect to the system of identical TPs. According to the Figure 11), the *AB* segment contains an extra vdW gap, whereas the *BA* segment miss one.

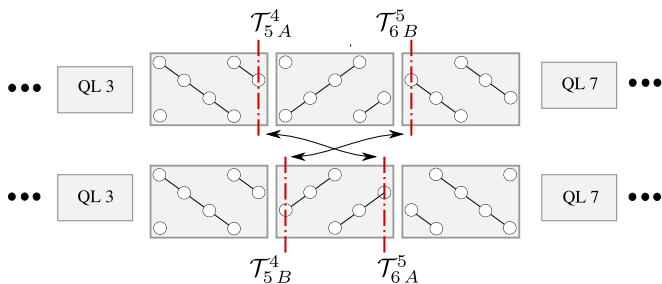


FIG. 11: Sketch of the interchange of the AB TP order with the BA one in the case of gathered TPs.

Except the case of the inverted middle TP (ABA), the calculated energy curves qualitatively resemble to the relative formation energy curve of identical TPs (Figure 10a). Namely, the BAA and AAA are nearly same. The observed disfavor of the AB order likely gives rise to a slightly higher slope of the AAB energy curve in comparison to the case of identical TPs. The relative increase of the formation energy might be ascribed to elongation of the segment between A - and B -typed TPs. The shape of ABA formation energy curve can be explained in the similar way. There occurs a local maximum of the relative formation energy as a function of the position of the middle TPs. It likely originates from a complex interplay arising from the occurrence of two diametrically opposite inter-TP segments AB and BA , while their length is modified.

Considering the symmetry of the Bi_2Se_3 slab placed into the vacuum, where the BAA order is equivalent to the BBA one by a side inversion, one might assume that such immediate alternation of the TP types (ABA) is unlikely based on the calculated formation energies. Hence, it appears that the role of the TPs orientation can be regarded as marginal concerning the distribution of TPs in the undoped structure.

The relative formation energies dramatically changes under the presence of the magnetic defects similarly to the case of the identical TPs (Figure 10b). Although the energy curves are modified by presence of distinct TPs, the local energy minima belonging to gathered TPs are kept. The presence of magnetic dopants reorders the formation energies according to the variation of the TPs orientation. It is likely related to the described interplay of TPs and the magnetic dopants (Figure 9). We show that the formation energy of TPs still grows with increased amount of the magnetic dopants nearly irrespective of the TPs positions (compare Figure 10c and Figure 6). The existing exceptions originating from the special order of TPs, where TPs are more favorable under magnetic doping (Figure 10b). Besides, one should be aware that the calculated curves (Figure 10c) are influenced by vacuum interface induced effects similar to the identical TPs (Figure 5). Finally, one can conclude that the TPs orientation does not cause significant qualitative changes in the TPs behavior even in the case of

magnetic disorder as the lowest energy case almost mimic the behavior of the system with identical TPs.

E. Surface states

Conductive Dirac surface states are one of the most interesting properties of TIs. The appearance of TPs can strongly influence their presence since the mirroring of the structure symmetry could represent a boundary in the structure. Hence, in this paper we also try to simulate the influence of the presence of TP and its position on the surface states. We calculated Bloch spectral functions (BSF) in the vicinity of the Γ point, where the Dirac cone exists, on the path between high symmetrical reciprocal points M and K . In order to study the band gap and surface states we project BSFs it along the mentioned $K - \Gamma - M$ path to the energy-intensity plane in a way that the maximal intensity of the BSF over the k -path is selected for particular energy points. Then, a formation of the Dirac states is indicated by vanishing of the energy gap and an occurrence of a strikingly high intensity at the Dirac point, where the surface states intersect (Figure 12a). The projected BSFs (PBSF) reveal that the presence of a TP in at a certain distance from the surface breaks the surface Dirac states, which exist in the unperturbed structure (Figure 12a). Our calculations showed that for TPs which are closer than 6 QLs to the surface a gap opens. In Figure 12a it appears especially under presence of \mathcal{T}_4^3 . The oscillations occurring in PBSF dependencies are caused by finite energy- and k -mesh, which prevents obtaining smooth electron bands in terms of the BSF as well as a narrow k -window, which cuts energy bands. Energy scales are related to the position of the well defined conduction band edge (E_{cb}) at an inner QL (Figure 12b). As it was mentioned the observed canceling of surface states and gap opening likely arise from the proximity of two interfaces, which leads to a destructive interference [6]. Comparing results obtained for TP below the seventh QL with the unperturbed system we found almost no difference as the Dirac cone is recovered. Similarly, one can mention a modulation of the bulk band gap width in the vicinity of a TP (Figure 12b), where a band gap width changes due to the presence of a boundary.

IV. CONCLUSIONS

We have studied the behavior of TPs in pure layered Bi_2Se_3 system as well as in Bi_2Se_3 under the presence of magnetic and nonmagnetic disorder by first principles calculations. Calculating total energies of various distributions of several TPs in the multilayer structure, we evaluated the interaction energy between TPs in dependence on the state of doping. It shows that interaction between TPs in the pure Bi_2Se_3 becomes negligible for distances above three QLs. However, for smaller dis-

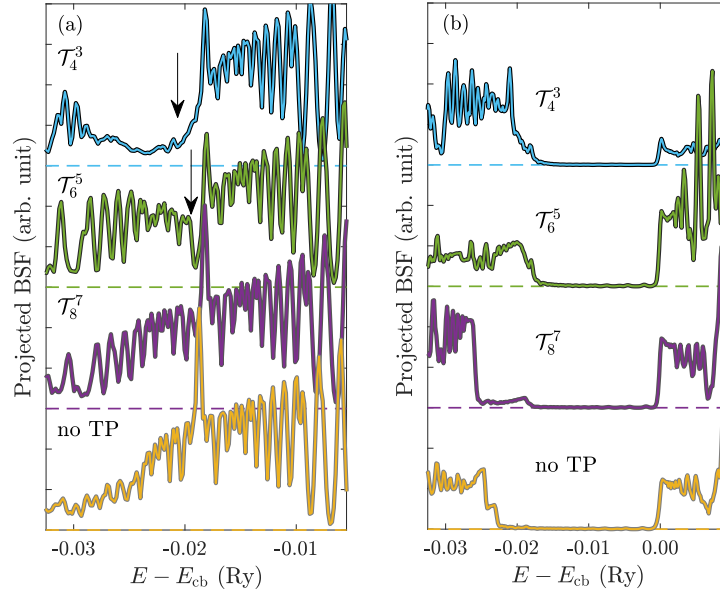


FIG. 12: Projected BSF of pure Bi_2Se_3 in the vicinity of Γ point in dependence on the position of TP. Spin up and spin down channels are overlaying. Obtained surface gaps are denoted by arrows. (a) PBSF of the surface QL, (b) PBSF of the fifth QL from the surface. Energy axis are scaled to the position of conduction band edge E_{cb} at the fifth QL.

tances a significant increase of the TP formation energy was observed, in agreement with the experimentally observed spatial separation of TPs in real samples. The influence of TPs on the surface states of pure Bi_2Se_3 was also studied. We have shown that the surface gap is opened if a TP is closer to it than 6nm.

The distribution of TPs and their interplay significantly changes under presence of chemical disorder. The presence of non-magnetic disorder weakens the influence of TPs on the electron structure and therefore the interactions between TPs are significantly smaller. However, the occurrence of magnetic defects modified the behavior of TPs significantly. Calculations revealed that adjacent TPs are energetically more favorable, which corresponds to the dependence of the relative formation energy of TPs on the concentration of magnetic doping. It reflects a suppression of the TPs formation in magnetically doped structures, unlike Bi antisites which increase the tendency to TP formation. Gathering of TPs leads to a smaller total perturbation of the electron structure and hence might be comprehended as a tendency to TPs annihilation. A thorough analysis indicates that the observed mismatch between the magnetic doping and the presence of TPs consists in the influence of TPs on the spin splitting of magnetic atoms.

On the other hand, variation of spin splitting, caused by TPs, influence a site preference of magnetic defects within the structure. There occur energetically either more or less preferred sites in the vicinity of the stacking fault, which can be related to the observed variation of magnitudes of magnetic moments of dopants through the simulated slab. Mn generally does not prefer to occupy

sites right at the twin boundary according to our calculations. Such behavior is indicated also in experiments, since no metallic Mn-Mn bonds were observed while they would probably arise if clustering of Mn at these boundaries was present [42]. For some sites in the immediate vicinity the energy was lowered, hence the concentration there could be higher than average in the sample.

ACKNOWLEDGEMENT

This research was funded the Czech Science Foundation (Grant No. 19-13659S). Access to computing and storage facilities owned by parties and projects contributing to the National Grid Infrastructure MetaCentrum provided under the programme “Projects of Large Research, Development, and Innovations Infrastructures” (CESNET LM2015042), is greatly appreciated. This work was supported by The Ministry of Education, Youth and Sports from the Large Infrastructures for Research, Experimental Development and Innovations project “e-Infrastructure CZ – LM2018140”

Appendix: Single TP distribution

To check behavior of a single TP in a pure multilayer structure and to discuss the vacuum interface caused effect, a distribution of the single TP in a multilayer consisting of 10 QLs is studied. Thus, an asymmetric dependence of the relative TP formation energy as the function of the TP position was obtained (Figure 13a). According

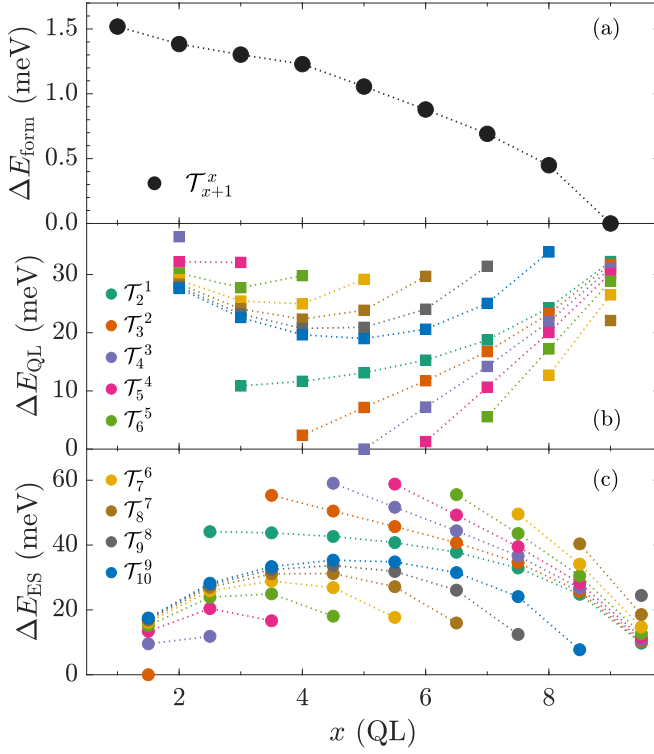


FIG. 13: (a) Single TP relative formation energy ΔE_{form} as a function of the position of TP x in the Bi_2Se_3 multilayer. (b) Relative energy contribution ΔE_{QL} of the particular QL x . (c) Relative energy contribution of ES in dependence on their position. Bi_2Se_3 multilayer consists of 10 QLs. Concerning plots (b) and (c), dependencies belonging to several locations of TPs are depicted, where data points in the vicinity of TPs are excluded for clarity.

to the Figure 2 a TP occurs at Se sites in the vicinity of vdW gap. Generally, one is used to dividing a system to twin domains adjacent to the twin boundary. However, according to the structure composed of QLs, we hypothetically split the present system into two domains separated by a vdW gap. It seems to be more convenient to deal with entire QLs in energy comparisons. Nevertheless, one has to be aware that one of domains contains a mirror layer. Since we used layer stacking according Figure 2, a TP is located in the domain bearing smaller QL indices. The relative formation energy (Figure 13a) bears a monotonous dependence, which favors a width maximization of the domain, where the mirror layer belongs. It suggests a significant interplay of the TP with the surface interfaces, which depends on the orientation of the TP.

Naturally, the occurrence of a TP in the structure causes a charge transfer compared to the unperturbed system. Calculations show (Figure 14) that the electron density changes primarily in the QL possessing a mirror plane of the Bi_2Se_3 layer stacking. Especially, the charge is depleted from the vdW gap and it flows to the Bi layer adjacent to the TP located at Se sites. Besides, a TP causes charge oscillations, which spread out of the TP. Evaluating the absolute charge transfer $\sum |\Delta \rho_t|^2$ per a domain based on the charge transfer distribution belonging to the system with symmetrical domain sizes (Figure 14), one finds that for the present way of stacking (Figure 2) the charge modulation is larger for the domain consisting of QLs with smaller indices. The difference is about one order of magnitude, which implies a different impact on domains. Having considered also vacuum interfaces, which represent another structure fault, the system naturally should tend to a suppression of the energetically more demanding perturbations by their separation (Figure 13a).

Let consider QLs and ES's separately and evaluate their relative total energy contributions. One observes that there occurs a clear discrepancy between the two presented domains regardless of the TP position. Relative magnitudes of total energies ΔE_{QL} related to particular QLs x as a function of the position of the TP display that the domain containing the TP, namely QLs with the smaller indices, possesses higher ΔE_{QL} and also the closer a TP to vacuum is the higher the magnitude of ΔE_{QL} is. For brevity, we exclude QLs in the vicinity of the TP, since their relative energy changes are of a different scale. Similarly, relative energy contributions of ES's (ΔE_{ES}) are also influenced by the position of the TP (Figure 13c). However, they follow an opposite evolution compared to the energy contribution of QLs likely because of an opposite impact of the stacking fault. The charge transfer of the related QLs and ES's differs in the sign. The formation energy curve (Figure 13a) includes both contributions, ΔE_{QL} and ΔE_{ES} . However, we observe that the shape of the formation energy curve ΔE_{form} (Figure 13a) is mostly determined by ES's contribution ΔE_{ES} (Figure 13c).

It is worthy to study the influence of a single TP on surrounding atomic layers in a pristine structure as it describes a bare effect of a TP. It shows that the perturbation caused by a TP is hardly local. Dependencies of the charge transfer (Figure 14) or the QL resolved total energy (Figure 13c) indicate that the charge as well as energy modulation spread over few QL. Moreover, a strong interplay with the Bi_2Se_3 boundaries is visible as it likely yields the shape of the E_{form} dependence (Figure 13a).

[1] A. Bansil, H. Lin, and T. Das, Colloquium: Topological band theory, *Rev. Mod. Phys.* **88**, 021004 (2016).

[2] Y. Xia, D. Qian, D. Hsieh, L. Wray, A. Pal, H. Lin, A. Bansil, D. Grauer, Y. S. Hor, R. J. Cava, and M. Z.

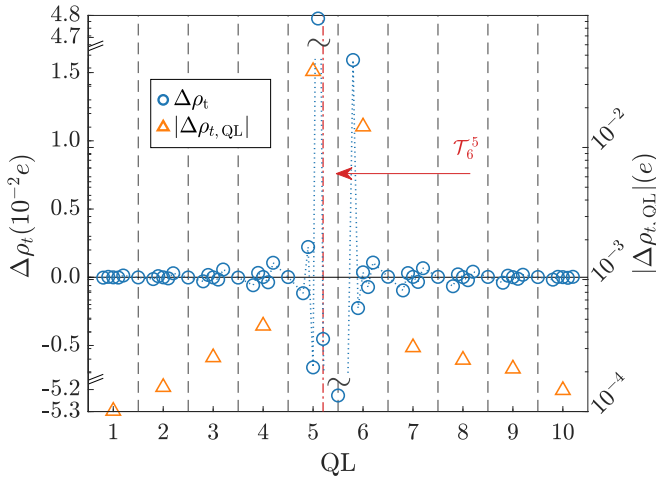


FIG. 14: (left axis) Distribution of the charge transfer $\Delta\rho_t$ caused by the presence of a twin plane (T_6^5) in the multilayer composed of 10 Bi_2Se_3 QLs. Each data point denotes a particular atomic layer or an ES representing the vdW gap. (right axis) Dependence of the variance of the charge transfer at particular QLs. Dashed lines separate QLs and denote position of the vdW gap.

Hasan, Observation of a large-gap topological-insulator class with a single dirac cone on the surface, *Nature Physics* **5**, 398 EP (2009).

- [3] X.-L. Qi and S.-C. Zhang, Topological insulators and superconductors, *Rev. Mod. Phys.* **83**, 1057 (2011).
- [4] D. Hsieh, Y. Xia, D. Qian, L. Wray, F. Meier, J. H. Dil, J. Osterwalder, L. Patthey, A. V. Fedorov, H. Lin, A. Bansil, D. Grauer, Y. S. Hor, R. J. Cava, and M. Z. Hasan, Observation of time-reversal-protected single-dirac-cone topological-insulator states in Bi_2Te_3 and Sb_2Te_3 , *Phys. Rev. Lett.* **103**, 146401 (2009).
- [5] M. Z. Hasan and C. L. Kane, Colloquium: Topological insulators, *Rev. Mod. Phys.* **82**, 3045 (2010).
- [6] Y. Zhang, K. He, C.-Z. Chang, C.-L. Song, L.-L. Wang, X. Chen, J.-F. Jia, Z. Fang, X. Dai, W.-Y. Shan, S.-Q. Shen, Q. Niu, X.-L. Qi, S.-C. Zhang, X.-C. Ma, and Q.-K. Xue, Crossover of the three-dimensional topological insulator Bi_2Se_3 to the two-dimensional limit, *Nature Physics* **6**, 584 EP (2010).
- [7] J. Cayssol, Introduction to dirac materials and topological insulators, *Comptes Rendus Physique* **14**, 760 (2013), topological insulators / Isolants topologiques.
- [8] B. Bernevig and T. Hughes, *Topological Insulators and Topological Superconductors* (Princeton University Press, New Jersey, USA, 2013).
- [9] F. Ortmann, S. Roche, and S. Valenzuela, *Topological Insulators: Fundamentals and Perspectives* (Wiley-VCH, Weinheim, Germany, 2015).
- [10] M. König, S. Wiedmann, C. Brüne, A. Roth, H. Buhmann, L. W. Molenkamp, X.-L. Qi, and S.-C. Zhang, Quantum spin hall insulator state in hgte quantum wells, *Science* **318**, 766 (2007), <https://science.sciencemag.org/content/318/5851/-766.full.pdf>.
- [11] L. A. Wray, S.-Y. Xu, Y. Xia, D. Hsieh, A. V. Fedorov, Y. S. Hor, R. J. Cava, A. Bansil, H. Lin, and M. Z. Hasan, A topological insulator surface under strong coulomb, magnetic and disorder perturbations, *Nature Physics* **7**, 32 EP (2010).
- [12] S.-Y. Xu, M. Neupane, C. Liu, D. Zhang, A. Richardella, L. Andrew Wray, N. Alidoust, M. Leandersson, T. Balasubramanian, J. Sánchez-Barriga, O. Rader, G. Landolt, B. Slomski, J. Hugo Dil, J. Osterwalder, T.-R. Chang, H.-T. Jeng, H. Lin, A. Bansil, N. Samarth, and M. Zahid Hasan, Hedgehog spin texture and berry's phase tuning in a magnetic topological insulator, *Nature Physics* **8**, 616 EP (2012), article.
- [13] C.-Z. Chang, J. Zhang, M. Liu, Z. Zhang, X. Feng, K. Li, L.-L. Wang, X. Chen, X. Dai, Z. Fang, X.-L. Qi, S.-C. Zhang, Y. Wang, K. He, X.-C. Ma, and Q.-K. Xue, Thin films of magnetically doped topological insulator with carrier-independent long-range ferromagnetic order, *Advanced Materials* **25**, 1065 (2013), <https://onlinelibrary.wiley.com/doi/pdf/10.1002/adma.201203493>.
- [14] K. Carva, J. Kudrnovský, F. Máca, V. Drchal, I. Turek, P. Baláz, V. Tkáč, V. Holý, V. Sechovský, and J. Honolka, Electronic and transport properties of the Mn-doped topological insulator Bi_2Te_3 : A first-principles study, *Phys. Rev. B* **93**, 214409 (2016).
- [15] F. Máca, J. Kudrnovský, P. Baláz, V. Drchal, K. Carva, and I. Turek, Tetragonal CuMnAs alloy: Role of defects, *Journal of Magnetism and Magnetic Materials* **474**, 467 (2019).
- [16] H. Zhang, C.-X. Liu, X.-L. Qi, X. Dai, Z. Fang, and S.-C. Zhang, Topological insulators in Bi_2Se_3 , Bi_2Te_3 and Sb_2Te_3 with a single dirac cone on the surface, *Nature Physics* **5**, 438 EP (2009), article.
- [17] W. Zhang, R. Yu, H.-J. Zhang, X. Dai, and Z. Fang, First-principles studies of the three-dimensional strong topological insulators Bi_2Te_3 , Bi_2Se_3 and Sb_2Te_3 , *New Journal of Physics* **12**, 065013 (2010).
- [18] Y. Lee, S. Punugupati, F. Wu, Z. Jin, J. Narayan, and J. Schwartz, Evidence for topological surface states in epitaxial Bi_2Se_3 thin film grown by pulsed laser deposition through magneto-transport measurements, *Current Opinion in Solid State and Materials Science* **18**, 279 (2014).
- [19] D. Kriegner, P. Harcuba, J. Veselý, A. Lesnik, G. Bauer, G. Springholz, and V. Holý, Twin domain imaging in topological insulator Bi_2Te_3 and Bi_2Se_3 epitaxial thin films by scanning X-ray nanobeam microscopy and electron backscatter diffraction, *Journal of Applied Crystallography* **50**, 369 (2017).
- [20] J.-M. Zhang, W. Ming, Z. Huang, G.-B. Liu, X. Kou, Y. Fan, K. L. Wang, and Y. Yao, Stability, electronic, and magnetic properties of the magnetically doped topological insulators Bi_2Se_3 , Bi_2Te_3 , and Sb_2Te_3 , *Phys. Rev. B* **88**, 235131 (2013).
- [21] Y. S. Hor, P. Roushan, H. Beidenkopf, J. Seo, D. Qu, J. G. Checkelsky, L. A. Wray, D. Hsieh, Y. Xia, S.-Y. Xu, D. Qian, M. Z. Hasan, N. P. Ong, A. Yazdani, and R. J. Cava, Development of ferromagnetism in the doped topological insulator $\text{Bi}_{2-x}\text{Mn}_x\text{Te}_3$, *Phys. Rev. B* **81**, 195203 (2010).
- [22] J.-M. Zhang, W. Zhu, Y. Zhang, D. Xiao, and Y. Yao, Tailoring magnetic doping in the topological insulator Bi_2Se_3 , *Phys. Rev. Lett.* **109**, 266405 (2012).
- [23] E. D. L. Rienks, S. Wimmer, J. Sánchez-Barriga, O. Caha, P. S. Mandal, J. Ruzicka, A. Ney, H. Steiner,

- V. V. Volobuev, H. Groiss, M. Albu, J. Kothleitner, G. and Michalicka, S. A. Khan, J. Minár, H. Ebert, G. Bauer, F. Freyse, A. Varykhalov, O. Rader, and G. Springholz, Large magnetic gap at the dirac point in $\text{Bi}_2\text{Te}_3/\text{MnBi}_2\text{Te}_4$ heterostructures, *Nature* **576**, 423 (2019).
- [24] Y. S. Hor, A. Richardella, P. Roushan, Y. Xia, J. G. Checkelsky, A. Yazdani, M. Z. Hasan, N. P. Ong, and R. J. Cava, p -type Bi_2Se_3 for topological insulator and low-temperature thermoelectric applications, *Phys. Rev. B* **79**, 195208 (2009).
- [25] D. O. Scanlon, P. D. C. King, R. P. Singh, A. de la Torre, S. M. Walker, G. Balakrishnan, F. Baumberger, and C. R. A. Catlow, Controlling bulk conductivity in topological insulators: Key role of anti-site defects, *Advanced Materials* **24**, 2154 (2012), <https://onlinelibrary.wiley.com/doi/pdf/10.1002/adma.201200187>.
- [26] A. Wolos, A. Drabinska, J. Borysiuk, K. Sobczak, M. Kaminska, A. Hruban, S. G. Strzelecka, A. Materna, M. Piersa, M. Romaniec, and R. Diduszko, High-spin configuration of mn in Bi_2Se_3 three-dimensional topological insulator, *Journal of Magnetism and Magnetic Materials* **419**, 301 (2016).
- [27] F.-T. Huang, M.-W. Chu, H. H. Kung, W. L. Lee, R. Sankar, S.-C. Liou, K. K. Wu, Y. K. Kuo, and F. C. Chou, Nonstoichiometric doping and bi antisite defect in single crystal bi_2se_3 , *Phys. Rev. B* **86**, 081104 (2012).
- [28] D. L. Medlin and N. Y. C. Yang, Interfacial Step Structure at a (0001) Basal Twin in Bi_2Te_3 , *Journal of Electronic Materials* **41**, 1456 (2012).
- [29] D. L. Medlin, Q. M. Ramasse, C. D. Spataru, and N. Y. C. Yang, Structure of the (0001) basal twin boundary in Bi_2Te_3 , *Journal of Applied Physics* **108**, 043517 (2010), <https://doi.org/10.1063/1.3457902>.
- [30] N. V. Tarakina, S. Schreyeck, M. Luysberg, S. Grauer, C. Schumacher, G. Karczewski, K. Brunner, C. Gould, H. Buhmann, R. E. Dunin-Borkowski, and L. W. Molenkamp, Suppressing twin formation in Bi_2Se_3 thin films, *Advanced Materials Interfaces* **1**, 1400134 (2014), <https://onlinelibrary.wiley.com/doi/pdf/10.1002/admi.201400134>.
- [31] I. Levy, T. A. Garcia, S. Shafique, and M. C. Tamargo, Reduced twinning and surface roughness of Bi_2Se_3 and Bi_2Te_3 layers grown by molecular beam epitaxy on sapphire substrates, *Journal of Vacuum Science & Technology B* **36**, 02D107 (2018), <https://doi.org/10.1116/1.5017977>.
- [32] H. Aramberri, J. I. Cerdá, and M. C. Muñoz, Tunable dirac electron and hole self-doping of topological insulators induced by stacking defects, *Nano Letters* **15**, 3840 (2015).
- [33] H. L. Skriver, *The LMTO Method: Muffin-Tin Orbitals and Electronic Structure* (Springer, Berlin, 2012).
- [34] I. Turek, V. Drchal, J. Kudrnovsky, M. Sob, and P. Weinberger, *Electronic Structure of Disordered Alloys, Surfaces and Interfaces* (Kluwer, Boston, 1997).
- [35] S. H. Vosko, L. Wilk, and M. Nusair, Accurate spin-dependent electron liquid correlation energies for local spin density calculations: a critical analysis, *Canadian Journal of Physics* **58**, 1200 (1980), <https://doi.org/10.1139/p80-159>.
- [36] P. A. Korzhavyi, A. V. Ruban, I. A. Abrikosov, and H. L. Skriver, Madelung energy for random metallic alloys in the coherent potential approximation, *Phys. Rev. B* **51**, 5773 (1995).
- [37] B. Velický, S. Kirkpatrick, and H. Ehrenreich, Single-site approximations in the electronic theory of simple binary alloys, *Phys. Rev.* **175**, 747 (1968).
- [38] J. Kudrnovský, V. Drchal, C. Blaas, P. Weinberger, I. Turek, and P. Bruno, Ab initio theory of perpendicular magnetotransport in metallic multilayers, *Phys. Rev. B* **62**, 15084 (2000).
- [39] I. Turek, J. Kudrnovský, M. Šob, V. Drchal, and P. Weinberger, Ferromagnetism of imperfect ultrathin Ru and Rh films on a $\text{ag}(001)$ substrate, *Phys. Rev. Lett.* **74**, 2551 (1995).
- [40] J. Kudrnovský, V. Drchal, I. Turek, P. Dederichs, P. Weinberger, and P. Bruno, Ab initio theory of perpendicular transport in layered magnetic systems, *Journal of Magnetism and Magnetic Materials* **240**, 177 (2002), 4th International Symposium on Metallic Multilayers.
- [41] F. H. Spedding, A. H. Daane, and K. W. Herrmann, The crystal structures and lattice parameters of high-purity scandium, yttrium and the rare earth metals, *Acta Crystallographica* **9**, 559 (1956).
- [42] M. Vališka, J. Warmuth, M. Michiardi, M. Vondráček, A. S. Nganheu, V. Holý, V. Sechovský, G. Springholz, M. Bianchi, J. Wiebe, P. Hofmann, and J. Honolka, Topological insulator homojunctions including magnetic layers: The example of n-p type (n-qls $\text{bi}_2\text{se}_3/\text{mn-bi}_2\text{se}_3$) heterostructures, *Applied Physics Letters* **108**, 262402 (2016), <https://doi.org/10.1063/1.4954834>.
- [43] K. Carva, P. Baláz, J. Šebesta, I. Turek, J. Kudrnovský, F. Máca, V. Drchal, J. Chico, V. Sechovský, and J. Honolka, Magnetic properties of Mn-doped Bi_2Se_3 topological insulators: Ab initio calculations, *Phys. Rev. B* **101**, 054428 (2020).
- [44] A. Liechtenstein, M. Katsnelson, V. Antropov, and V. Gubanov, Local spin density functional approach to the theory of exchange interactions in ferromagnetic metals and alloys, *Journal of Magnetism and Magnetic Materials* **67**, 65 (1987).
- [45] I. Turek, J. Kudrnovský, V. Drchal, and P. Bruno, Exchange interactions, spin waves, and transition temperatures in itinerant magnets, *Philosophical Magazine* **86**, 1713 (2006), <https://doi.org/10.1080/14786430500504048>.
- [46] A. Polyakov, H. L. Meyerheim, E. D. Crozier, R. A. Gordon, K. Mohseni, S. Roy, A. Ernst, M. G. Vergniory, X. Zubizarreta, M. M. Otrokov, E. V. Chulkov, and J. Kirschner, Surface alloying and iron selenide formation in $\text{Fe}/\text{Bi}_2\text{Se}_3(0001)$ observed by x-ray absorption fine structure experiments, *Phys. Rev. B* **92**, 045423 (2015).